1 **Secondary Organic Aerosols from OH Oxidation of Cyclic Volatile Methyl Siloxanes as an Important**

2 **Si Source in the Atmosphere**

3 Chong Han[1,2], Hongxing Yang[1], Kun Li[2,3], Patrick Lee[2], John Liggio[2], Amy Leithead[2], Shao-Meng Li[4*]

4 [1]School of Metallurgy, Northeastern University, Shenyang, 110819, China

5 [2]Air Quality Research Division, Environment and Climate Change Canada, Toronto, Ontario M3H 5T4,

6 Canada

7 [3]Laboratory of Atmospheric Chemistry, Paul Scherrer Institute, Villigen 5232, Switzerland

8 [4]State Key Joint Laboratory of Environmental Simulation and Pollution Control, College of Environmental

9 Sciences and Engineering, Peking University, Beijing, China 100871

10 **Correspondence**: Shao-Meng Li (shaomeng.li@pku.edu.cn)

11

12 **Short summary:** We presented yields and compositions of Si-containing SOA generated from the reaction

13 of cVMS (D3-D6) with OH radicals. NO_x played negative roles on cVMS SOA formation, while ammonium

14 sulfate seeds enhanced D3-D5 SOA yields at short photochemical ages under high-NO_x conditions. The

15 aerosol mass spectra confirmed that the components of cVMS SOA significantly relied on OH exposure. A

16 global cVMS-derived SOA source strength was estimated to understand SOA formation potentials of cVMS.

17

18 **Abstract**

19   Cyclic volatile methyl siloxanes (cVMS) are active ingredients in widely used consumer products, which

20 can volatilize into the atmosphere, thus attracting much attention due to their potential environmental risks.

21 While in the atmosphere the cVMS undergo oxidation yielding both gaseous and particulate products. The

22 aerosol yields and compositions from the OH oxidation of four cVMS (D3-D6) were determined under low

23 and high-NO$_x$ conditions in an oxidation flow reactor. The aerosol yields progressively increased from D3

24 to D6, consistent with the volatilities and molecule weights of these cVMS. NO$_x$ can restrict the formation

25 of SOA, leading to lower SOA yields under high-NO$_x$ conditions than under low-NO$_x$ conditions, with a

26 yield decrease between 0.05-0.30 depending on the cVMS. Ammonium sulfate seeds exhibited minor

27 impacts on SOA yields under low-NO$_x$ conditions, but significantly increased the SOA yields in the oxidation

28 of D3-D5 at short photochemical ages under high-NO$_x$ conditions. The mass spectra of the SOA showed a

29 dependence of its chemical compositions on OH exposure. At high exposures, equivalent to photochemical

30 ages of >6 days in the atmosphere, D4-D6 SOA mainly consisted of C$_x$H$_y$ and C$_x$H$_y$O$_z$Si$_n$ under low-NO$_x$

31 conditions, whereas they primarily contained N$_m$O$_z$, C$_x$H$_y$, C$_x$H$_y$O$_1$, C$_x$H$_y$O$_{>1}$ and C$_x$H$_y$O$_z$Si$_n$ under high-NO$_x$

32 conditions. The potential contributions of cVMS to SOA formation in the atmosphere were evaluated using

33 the reported cVMS annual production and the yield data obtained at the longest equivalent days in the present

34 study. A global cVMS-derived SOA source strength is estimated to be 0.16 Tg yr^{-1}, distributed over major

35 urban centers.

36

37 **1 Introduction**

38　　Secondary organic aerosols (SOA), which contribute 50-85% to the mass of atmospheric organic aerosols

39 (OA) (Glasius and Goldstein, 2016), are mainly formed via the partitioning of low volatility products from

40 oxidation of volatile organic compounds (VOCs), semi- and intermediate volatile organic

41 compounds(S/IVOCs) (Riipinen et al., 2012). SOA has attracted significant attention due to their important

42 impacts on climate, ecosystems and human health (Berndt et al., 2016). Global budgets of SOA remain an

43 unresolved issue despite extensive research, largely due to uncertainties associated with aerosol yields and

44 the presence of unconsidered SOA precursors.

45   As one type of anthropogenic VOC and potential SOA precursors, cyclic volatile methyl siloxanes (cVMS)

46   are widely used in industrial applications and personal care products (Genualdi et al., 2011; Krogseth et al.,

47   2013a). cVMS have been classified as high-volume chemicals with an annual production of millions of tons

48   globally (Rücker and Kümmerer, 2015; Ahrens et al., 2014). Studies of cVMS in the environment have

49   focused on investigating health and environmental impacts particularly due to their potential persistence,

50   bioaccumulation and toxicity (Guo et al., 2019; Liu et al., 2018; Farasani and Darbre, 2017; Xu et al., 2019;

51   Kim et al., 2018; Coggon et al., 2018). As a result, the European Council has proposed a restriction on the

52   octamethylcyclotetrasiloxane (D4) and decamethylcyclopentasiloxane (D5) content in wash-off personal

53   care products to a limit of 0.1 mass% by 2020 (Eur-Lex, 2018). The legislative actions notwithstanding,

54   knowledge of environmental behavior of cVMS still needs to be further deepened as compared to their

55   applications and economic significance (Rücker and Kümmerer, 2015).

56   It has been estimated that approximately 90% of cVMS are emitted into the atmosphere due to their high

57   saturation vapor pressures (Allen et al., 1997). Gas-phase cVMS have been observed in both indoor and

58   outdoor air. Tang et al. (2015) reported that cVMS accounted for about one third of total VOC mass

59   concentration in a classroom. Outdoor air concentrations of cVMS have also been measured at different sites

60   worldwide (Li et al., 2020; Wang et al., 2018; Rauert et al., 2018), increasing from rural to urban sites and

61   consistent with increasing population density (Rücker and Kümmerer, 2015). For example, at a rural site in

62   Sweden, the concentration of hexamethylcyclotrisiloxane (D3), D4, D5 and dodecamethylcyclohexasiloxane

63   (D6) were 0.94, 3.5, 13 and 1 ng/m^3, respectively (Kierkegaard and Mclachlan, 2013), while they were 18,

64   55, 172 and 14 ng/m^3 in urban areas of Toronto in Canada, respectively (Genualdi et al., 2011; Rauert et al.,

65   2018). cVMS have also been detected in the remote Arctic atmosphere, confirming their long-range transport

66   (Genualdi et al., 2011; Krogseth et al., 2013b). Atmospheric half-lives of cVMS are on the order of 30, 15,

67   10 and 6 days for D3-D6, respectively, which allow cVMS to exhibit a hemispherical distribution in the

68   atmosphere (Canada, 2008; Xiao et al., 2015). These lifetimes are driven mostly by reactions with the OH

69   radicals (Xiao et al., 2015; Wang et al., 2013), which generate silanols and dimeric products that can be

70   partitioned to condensed phases (Coggon et al., 2018; Sommerlade, 1993; Wu and Johnston, 2016). Different

71   OH concentrations can partly explain the seasonal variation of cVMS lifetimes that was characterized by

72   longer during winter than in summer (Rücker and Kümmerer, 2015). The loss of cVMS in the atmosphere is

73   negligible through O_3 and NO_3 due to their small reaction rates (Atkinson, 1991). The global loss by the

74   reaction with Cl atoms is less than 5 % on account of low Cl concentrations, although it may be higher in

75   some regions where cVMS emissions and Cl sources overlap in both space and time (Alton and Browne,

76   2020). It has been demonstrated that elemental Si is a frequent constituent of nanoparticles in rural and urban

77   areas (Phares et al., 2003; Rhoads, 2003; Bein, 2005; Bzdek et al., 2014) and in remote regions (Li and

78   Winchester, 1990; Li and Winchester, 1993). These Si-containing nanoparticles have previously been

79   attributed to ore smelting processes, but recent studies have shown that Si-containing species are one of the

80   main components in cVMS SOA, suggesting that the oxidation of cVMS may be an important source of Si

81   in atmospheric aerosols (Wu and Johnston, 2016, 2017). In a modeling study, the oxidation products of

82   cVMS (D4, D5 and D6) were considered to quantify the maximum potential for aerosol formation through

83   reactions with the OH radicals (Janechek et al., 2017). Chandramouli and Kamens (2001) demonstrated the

84   gas-particle partitioning of silanols from D5 oxidation by the OH radicals. Wu and Johnston (2016, 2017)

85   analyzed the chemical composition of secondary aerosols from OH oxidation of D4 and D5, showing a large

86   number of monomeric and dimeric products. Janechek et al. (2017, 2019) reported physical properties of

87   SOA generated by OH oxidation of D5, including hygroscopicity, cloud seeding potential and volatility.

88   Charan et al. (2022) measured SOA yields of D5 using chambers and flow tube reactors, emphasizing the

89   importance of the relevant OH concentrations and exposures when extrapolating these laboratory results or

90   comparing with other studies. These studies mainly focused on D5 and occasionally D4 but rarely others. To

91   better understand the SOA-forming potentials of typical cVMS in the atmosphere, accurate yields and

92   molecular compositions of SOA from the oxidation of cVMS under various atmospheric conditions are

93   needed.

94   In this work, the formation of SOA from the oxidation of four cVMS (D3-D6) by OH radical was

95   investigated in an oxidation flow reactor (OFR). Under various combinations of NO_x and ammonium sulfate

96   seed concentrations, the yields and compositions of SOA formed from the oxidation were measured using a

97   suite of instruments including a scanning mobility particle sizer (SMPS), a proton transfer reaction time of

98   flight mass spectrometer (PTR-ToF-MS) and an aerosol mass spectrometer (AMS). Based on these SOA

99   yields, the contribution of cVMS to SOA in the global atmosphere was estimated using reported cVMS

100   concentrations. The results obtained here can largely improve our understanding of the contribution and

101   composition of SOA from cVMS.

102   **2 Experiments and methods**

103   **2.1 Photo-oxidation experiments**

104   The reactions of cVMS with OH radicals were controlled at a constant temperature (21±1˚C) and relative

105   humidity (35%±2%) in a custom-made oxidation flow reactor (the Environment and Climate Change Canada

106   oxidation flow reactor, ECCC-OFR), which is shown in Fig. S1 of the Supplement and has been described

107   in detail previously (Li et al., 2019a). Briefly, the ECCC-OFR is a fused quartz cylinder (length: 50.8 cm,

108   inner diameter: 20.3 cm) equipped with a conical inlet and 7 outlets. Wall losses of particles and gases in the

109   ECCC-OFR have been shown to be lower than in other OFRs (Huang et al., 2017; Lambe et al., 2011;

110   Simonen et al., 2017; Li et al., 2019a). The length and full angle of cone inlet are 35.6 cm and 30°,

111 respectively, designed to minimize the formation of jetting and recirculation in the OFR. The outlet at the

112 reactor center is a stainless-steel sampling port (inner diameter: 0.18 in) extending 12.7 cm long into the

113 ECCC-OFR. This sampling inlet reduces the impact of potential turbulent eddies caused by the back end of

114 the reactor. The remaining 6 outlets around the perimeter are designed to allow side flows to pass through

115 the OFR as a sheath flow, indirectly reducing wall losses of gases and particles inside the OFR upon sampling.

116 Ozone-free mercury UV lamps for generating OH radicals are housed in small quartz tubes around and in

117 parallel to the quartz reaction cylinder, and a large flow of air through each of these smaller quartz tubes is

118 used to remove the heat produced by the lamps. The relative humidity was adjusted by controlling the ratio

119 of dry air to wet air into the reactor, and was measured using a humidity sensor (Vaisala) at one of the sheath

120 flow outlets (side flows) of the reactor. The volume of the entire ECCC-OFR is about 16 L and the total flow

121 rate is 8 L min^{-1}, leading to a residence time of 2 min in the OFR.

122   OH radicals were produced through the reaction of water vapor with O(^{1}D) formed from O$_3$ photolysis at

123 254 nm. The OH concentration in the ECCC-OFR was regulated by controlling the input voltage and the

124 number of UV lamps. Methanol vapor, introduced into the ECCC-OFR through a bubbler containing

125 methanol solution, was used to determine the OH exposure (i.e., photochemical age, from the multiplication

126 of OH concentration and reaction time) by tracking its decay in the reactor from the reaction with the OH.

127 The decay, or fractional loss, of gas-phase methanol, [MeOH]/[MeOH]$_0$ was measured with the PTR-ToF-

128 MS, and was used to calculate the OH concentration via Equation 1,

129 $$[OH]=-\frac{1}{k_{MeOH}} \ln \frac{[MeOH]}{[MeOH]_0}$$ (1)

130 where k$_{MeOH}$ is the second-order rate constant of methanol reaction with OH at 298 K (9.4×10^{-13} cm^3

131 molecule^{-1} s^{-1}). It was noted that the OH exposure measurement was offline, because methanol can affect the

132 OH reactivity with cVMS. Under low and high-NO$_x$ conditions described below, the OH exposure varied in

133   the range of 5.5×10^{10}-1.8×10^{12} and 8.2×10^{10}-1.1×10^{12} molecules cm^{-3} s, respectively. They correspond

134   to 0.4-14.2 and 0.6-8.5 equivalent days (photochemical age), respectively, assuming that an average OH

135   concentration in air is 1.5×10^6 molecules cm^{-3} (Mao et al., 2009).

136   Pure D3-D6 cVMS compounds (solid D3 and liquid D4, D5 and D6) were placed in a glass U-type tube

137   and maintained at the room temperature. Vapors from these compounds (Table S1 of the Supplement) were

138   separately introduced into the ECCC-OFR by a small flow of zero air (1-18 mL min^{-1}) passing over the

139   headspace of the U-tube containing the pure compounds. The concentrations of D3-D6 in the ECCC-OFR

140   ranged from 20 to 43 ppb (Table S2), depending on their volatilities. Table S2 summarizes the concentrations

141   of cVMS at the reactor inlet and outlet, when the OH exposure was 1.85×10^{12} and 1.10×10^{12} molecules cm^{-}

142   ^{3} s in low and high-NO_x experiments, respectively, indicating the reaction depth of cVMS. To study the

143   influence of existing particles on the SOA formation, ammonium sulfate (AS) seed particles were produced

144   using an atomizer, dried by a diffusion dryer and neutralized by a neutralizer and injected into the reactor

145   without size selection. The mass concentration of AS seed particles was approximately 30 μg m^{-3} for all

146   experiments.

147   N_2O was used as a source of NO to achieve high-NO_x conditions (Lambe et al., 2017). NO_x conditions

148   were defined by the fate of peroxy radicals (RO_2), which was described by the reaction rate ratio (R_{NO}) of

149   RO_2 + NO and RO_2 + HO_2 (Peng et al., 2018). The R_{NO} ratio increases with increasing OH exposures at a

150   constant concentration of N_2O (Li et al., 2019b). To achieve a constant branching ratio during the high-NO_x

151   experiments, the initial N_2O concentration in the OFR was varied (1.6%-8.0%) to maintain an R_{NO} value of

152   20 (Li et al., 2019b), as calculated using a model (OFR Exposures Estimator v3.1) (Peng et al., 2018). A

153   ratio of R_{NO}=20 indicates that 95% of RO_2 reacts with NO, ensuring the dominance of RO_2 + NO, which

154   represents conditions that are relevant for urban atmosphere (Peng et al., 2019). The role of RO_2 + RO_2 here

155   should be minor or negligible due to the low concentration of SOA precursors (cVMS, 18-46 ppb) (Lambe

156   et al., 2017; Peng et al., 2019; Li et al., 2019b). Peng et al. (2019) have reported that in the experiments

157   utilizing the injection of N_2O to achieve high-NO_x conditions, the relative importance of $RO_2 + OH$ was

158   generally negatively correlated with N_2O due to the suppressing effect of NO_x on OH radicals and the

159   increasing role of $RO_2 + NO$. Under low-NO_x conditions, N_2O was not introduced into the OFR, where the

160   reaction ratio of RO_2 with HO_2 was estimated to be larger than 99% according to the model mentioned above

161   (Peng et al., 2018), representing atmospheric scenarios with few NO_x sources.

162   **2.2 Characterization and analysis**

163   The concentrations of cVMS in the OFR were measured online with PTR-ToF-MS (Ionicon Analytik

164   GmbH) (Liggio et al., 2016). The number and mass size distribution of aerosols was monitored using a

165   scanning mobility particle sizer (SMPS, TSI). The mass spectra and elemental composition of aerosols was

166   determined with a high-resolution time-of-flight aerosol mass spectrometer (HR-ToF-AMS, Aerodyne) and

167   analyzed with the AMS analysis software Squirrel (version 1.62G) and Pika (version 1.22G).

168   SOA mass yields (*Y*) were calculated via Equation 2,

169
$$Y = \frac{\Delta C_{\text{SOA}}}{\Delta C_{\text{cVMS}}} \tag{2}$$

170   where ΔC_{SOA} and ΔC_{cVMS} are the mass concentrations of SOA formed and cVMS lost, respectively. The mass

171   concentration of SOA was determined by multiplying the effective aerosol density by the integrated SOA

172   volume concentration from the SMPS, subtracting the AS seed volume for experiments with AS seeds. The

173   effective aerosol density (ρ) was calculated for unseeded experiments through the following Equation 3

174   (Lambe et al., 2015),

175
$$\rho = \frac{D_{va}}{D_m} \tag{3}$$

176   where D_{va} is the vacuum aerodynamic diameter obtained from the HR-ToF-AMS, and D_m is the electric

177   mobility diameter measured by the SMPS. The ρ varied in the range of 1.6-1.8 depending on the cVMS. The

178   same ρ value was also used in the seeded experiments. It should be pointed out that the background values

179   in Table S3 have been subtracted when calculating the cVMS SOA yields. The average data of SMPS and

180   AMS in the last ~10 minutes for each OH exposure was used to calculate the SOA yields (inset of Fig S2),

181   which can reduce the deviation caused by unstable SOA loadings at high OH exposures.

3 Results and discussion

3.1 SOA yields

184   Taking the D5 SOA under unseeded conditions as an example, the number and mass size distributions of

185   aerosols were shown in Fig. S3 at three photochemical ages (PA), i.e., time-integrated OH exposure. It can

186   be seen that small particles dominated the total particle number counts, while large ones dominated the mass.

187   The mass mode diameter of SOA for mass size distributions increased with PA under low and high-NO_x

188   conditions. The mass concentrations and time series of SOA obtained from SMPS and AMS were shown in

189   Table S4 and Fig. S2, respectively, which reflected a step-by-step pattern with increasing OH exposures.

190   Unstable SOA loadings at high OH exposures may be attributed to the fragmentation reactions, leading to

191   the difficulty in the deposition of products on SOA.

192   Figure 1 shows the SOA yields from the photooxidation of the D3-D6 cVMS under low and high-NO_x

193   conditions as a function of PA, with and without AS seed particles. SOA yields have been widely used to

194   estimate the potential of precursors to produce aerosol mass (Mcfiggans et al., 2019; Li et al., 2019a; Bruns

195   et al., 2015; Lambe et al., 2015). As shown in Fig. 1, the cVMS SOA yields exhibited an overall increasing

196   trend with PA, expressed in equivalent photochemical days, which agreed with the trend of D5 SOA yields

197   reported by Janechek et al. (2019). Under low-NO_x conditions (Fig. 1a), SOA yields exhibited a slow growth,

198   reaching a plateau after 10 equivalent days. This may be due to increased gas-phase fragmentation of cVMS

199   to generate some higher volatility products, leading to a small increasing amplitude of partition ratio of

200   species into SOA at longer photochemical ages.
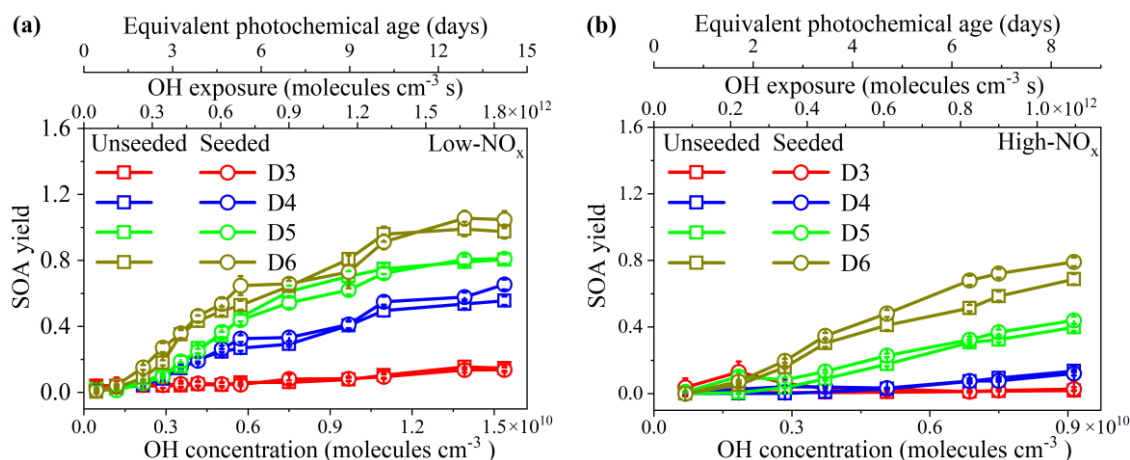
202   Figure 1. SOA yields from unseeded and seeded (30 μg m^{-3}) photooxidation of cVMS by OH radicals. **(a)**

203   low-NO$_x$ experiments; **(b)** high-NO$_x$ experiments.

204

205   For the unseeded and low-NO$_x$ experiments in Fig. 1a, SOA yields of four cVMS exhibited significant

206   differences in values over the same number of equivalent days. The SOA yields successively increased from

207   D3 to D6, consistent with the volatilities and molecular masses of the cVMS as well as their reaction rate

208   constants with the OH radical (Alton and Browne, 2020; Kim and Xu, 2017; Safron et al., 2015). The

209   maximum SOA yields of D3-D6 were (0.16±0.02), (0.56±0.03), (0.80±0.03) and (0.99±0.04), respectively,

210   occurring after a PA of 12 equivalent days. It has been reported that D5 SOA yields varied in the range of 0-

211   1.1 (Janechek et al., 2019; Wu and Johnston, 2017; Charan et al., 2022). Under a low OH exposure (~10^{10}-

212   10^{11} molecules cm^{-3} s), the D5 SOA yield (0.01-0.11) obtained here was similar to that (chamber, 0-0.057;

213   flow tube, 0.018-0.06) measured by Charan et al. (2022). However, under a high OH exposure of ~10^{11}-10^{12}

214   molecules cm^{-3} s, the D5 SOA yield of 0.46-0.70 was higher than 0.22 and 0.14-0.35 (flow tube) reported

215   by Janechek et al. (2019) and Charan et al. (2022), respectively, which may be attributed to differences in

216   experimental conditions, such as differences in reactors, wall losses, SOA measurement methods,

217   determination of OH concentrations, and initial D5 concentrations (Table S5) (Janechek et al., 2019; Charan

218   et al., 2022). Although the amount of cVMS lost was variable, cVMS SOA yields positively depended on

219   SOA mass concentrations (Fig. S4), and this trend was observed in previous D5 SOA experiments with OH

220   oxidation (Wu and Johnston, 2017).

221   As shown in Fig. 1b, the order of SOA yields from the four cVMS under high-NO_x conditions was the

222   same as that under low-NO_x conditions. However, the SOA yields under high-NO_x conditions were generally

223   smaller than the corresponding yields at similar OH exposures under low-NO_x conditions, with a decrease

224   of 0.05-0.30 depending on the cVMS. Such a reduction suggests that NO_x can restrict the formation of cVMS

225   SOA. NO_x has been shown to reduce SOA yields for some anthropogenic alkanes (Li et al., 2019b), aromatics

226   (Ng et al., 2007a; Chan et al., 2009; Zhou et al., 2019), monoterpenes (Zhao et al., 2018) and other terpenes

227   (Ng et al., 2007b), attributable to the formation of higher volatility products (e.g., organic nitrates) generated

228   by RO_2 + NO compared to RO_2 + HO_2 (Presto et al., 2005; Li et al., 2019b), which is also likely the case

229   here. The higher volatility products favor partitioning in the gas phase, thus reducing the potential for

230   forming SOA (Zhou et al., 2019). Moreover, high NO_x levels can suppress the formation of products for

231   nucleation, thereby reducing aerosol surface as a condensational sink and increasing the wall loss of

232   condensable species in an OFR under high-NO_x conditions (Zhao et al., 2018; Sarrafzadeh et al., 2016; Wildt

233   et al., 2014). Figure S5 indicates that the difference between SOA yields with and without NO_x decreased

234   with increasing silicon atoms within individual cVMS, indicating a less restricting effect of NO_x on the SOA

235   formation for larger cVMS. This means that high NO_x levels play a lessor role in the SOA yields of lower

236   volatility precursors.

237   SOA yields in the AS-seeded experiments under low and high-NO_x conditions are also shown in Figs. 1

238   and S5, indicating minimal impacts of the AS seed particles on SOA yields. A yield enhancement ratio

239   (R_E=Y_{seeded}/$Y_{unseeded}$, Fig. S6) was used to show the seed impacts more clearly. Under low-NO$_x$ conditions,

240   the R_E values for all cVMS were close to 1.0 (Fig. S6a), suggesting negligible impact of AS seed particles

241   on SOA yields; however, under high-NO$_x$ conditions, R_E was much larger (17.81, 13.18 and 15.51 for D3-

242   D5, respectively) at short PA but gradually decreased to 1.0 with increasing PA for D3-D5, while it was

243   always close to 1.0 for D6 regardless of PA (Fig. S6b). R_E values greater than 1.0 suggest that AS seed

244   particles played an enhancement role in the cVMS SOA formation, as similarly reported in SOA formation

245   from hydrocarbons (Sarrafzadeh et al., 2016; Lamkaddam et al., 2017; Li et al., 2019b). Under low-NO$_x$

246   conditions, the general lack of impact on cVMS SOA yields by the AS seed particles suggests that

247   condensation was not the main process driving SOA formation in cVMS oxidation. For the few cases of high

248   NO$_x$ level at low PA, where R$_E$ was >1 for D3-D5, it is possible that their early generations of oxidation

249   products were more volatile than successive generations of products and hence more prone to condensation

250   enhanced by AS seeds. As PA increased, further reactions of these early generation oxidation products with

251   OH radicals resulted in further generation products that were likely less volatile, thereby weakening the

252   enhancing role of AS seeds at high OH exposure. Such effect was less pronounced for D6, likely because its

253   oxidation products at different PA had similar volatilities. Figure S6b shows that the effect of AS seed

254   particles on SOA yields negatively correlated with the number of silicon atoms in the cVMS. Lower volatility

255   precursors (D5 and D6) may form lower volatile products, resulting in SOA yields less sensitive to the pre-

256   existing seeds. In fact, most D5 oxidation products have been shown to be nearly non-volatile (Janechek et

257   al., 2019; Wu and Johnston, 2017; Alton and Browne, 2020; Alton and Browne, 2022).

258   **3.2 Aerosol compositions**

259   **3.2.1 Compositions of SOA under low-NO$_x$ conditions.**

260   Figures 2 and S7 show the normalized HR-ToF-AMS mass spectra of cVMS SOA from unseeded

12

261   experiments under low-NO_x conditions at OH exposures of 9.0×10^{11} molecules cm^{-3} s (i.e., OH

262   concentration of 7.5×10^9 molecules cm^{-3}). The mass spectral signals can be identified as fragments with a

263   formula of $C_xH_yO_zSi_n$. For D3 SOA, the most prominent peaks were at m/z 44 and 29, dominated by CO_2^+

264   and CHO^+, which were tracers for organic acids (Ng et al., 2010), alcohols and aldehydes (Lee et al., 2012),

265   respectively. They may result from the oxidation of the methyl groups in D3 by OH radicals. For the mass

266   spectra of D4-D6 SOA, the two highest peaks at m/z 14 and 15 were CH_2^+ and CH_3^+, respectively. In addition,

267   there were several dominant $C_xH_yO_zSi_n$ peaks, which were fragments of silicon-containing products. For the

268     $C_xH_yO_zSi_n$ group in D4 SOA, there were four typical peaks at m/z 255, 257, 271 and 273, with formulae of

269     $C_4H_{11}O_7Si_3^+$, $C_3H_9O_8Si_3^+$, $C_3H_7O_9Si_3^+$ and $C_3H_9O_9Si_3^+$, respectively. The $C_xH_yO_zSi_n$ fragment group

270   containing Si of D5 SOA had three dominant peaks at m/z 327, 329 and 331, corresponding to $C_{12}H_{11}O_2Si_5^+$,

271     $C_9H_9O_8Si_3^+$ and $C_5H_{15}O_9Si_4^+$, respectively. For the $C_xH_yO_zSi_n$ group containing Si in D6 SOA, there were

272   five main peaks at m/z 73 (C_3H_9Si), 387 ($C_8H_{23}O_8Si_5^+$), 389 ($C_8H_9O_9Si_5^+$), 401 ($C_9H_{21}O_{10}Si_4^+$) and 403

273   ($C_7H_{15}O_{12}Si_4^+$).

274

275
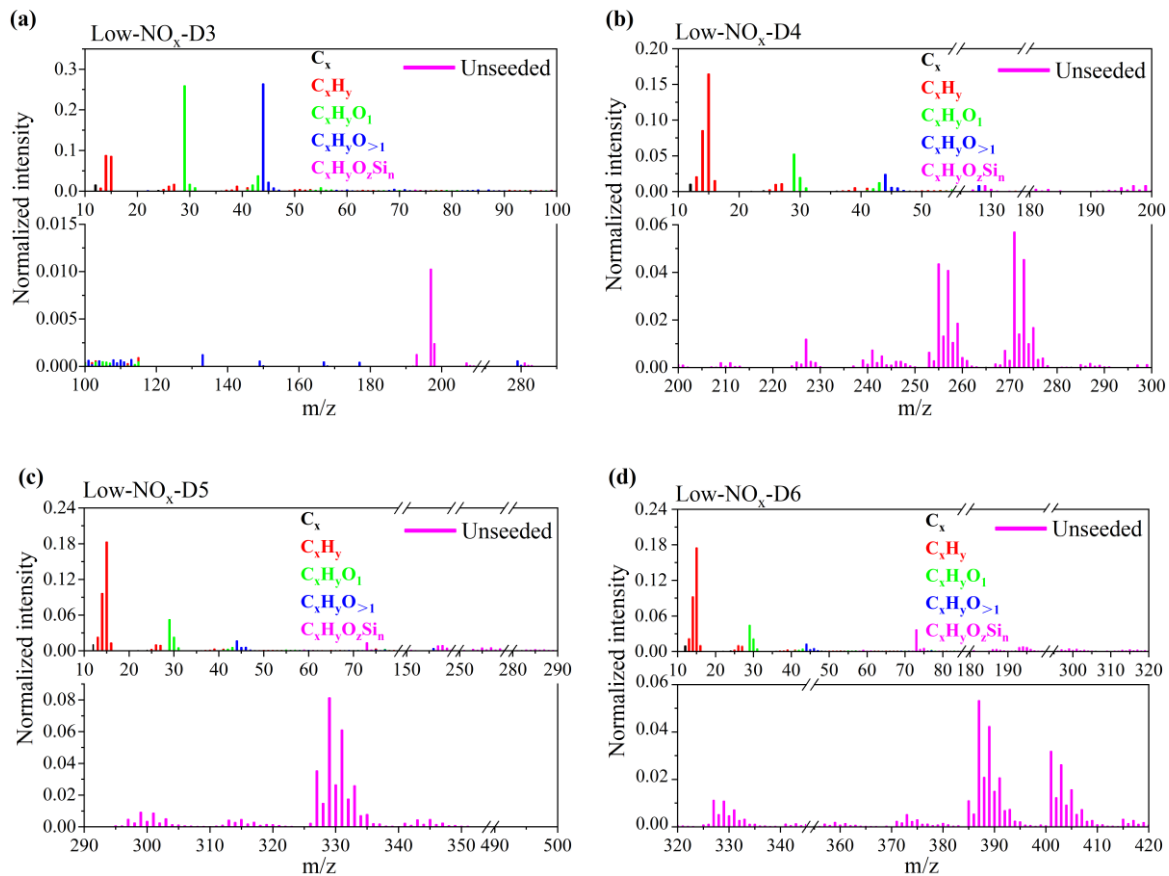
Figure 2. HR-ToF-AMS mass spectra of cVMS SOA at OH exposure of 9.0×10^{11} molecules cm^{-3} s (i.e.,

OH concentration of 7.5×10^9 molecules cm^{-3}) under low-NO$_x$ conditions in unseeded experiments. **a-d**

represent the mass spectra of D3-D6 SOA, respectively.

Figure 3 shows the evolution of different groups of ions in the HR-ToF-AMS spectra of the cVMS SOA

as a function of PA in equivalent days. For D3-D6 under unseeded conditions, $C_xH_yO_1$ and $C_xH_yO_{>1}$ ions

significantly decreased within 0-4 equivalent days of PA, but remained essentially unchanged when PA

increased to 7-15 equivalent days. The C_xH_y ion increased to its peak value at about 9 equivalent days of PA

for D3 and 2-3 equivalent days of PA for D4-D6, and then gradually decreased with further PA increases.

The $C_xH_yO_zSi_n$ group of ions maintained an increasing trend until 9-10 days of PA, thereafter it decreased

slightly for D4-D6 SOA.

287   The weighted values of the atomic number ratios Si/C (n/x) and Si/O (n/z) for the $C_xH_yO_zSi_n$ groups in

288   D5 and D6 SOA at different PA are plotted in Fig. S8 (Detailed calculations in Text S1 of the Supplement),

289   which can be used to indicate the changes in the Si element of SOA. The Si/C ratio at initial SOA formation

290   stage was close to that (0.50) in D5 and D6 molecules, and then increased continuously with increasing PA.

291   The Si/O ratio kept increasing from 0.53 to 1.15 for D5 SOA and from 0.72 to 1.32 for D6 SOA, but varying

292   around 1.0 that was the Si/O ratio in D5 and D6. While it is difficult to separate the effect of fragmentation

293   due to the AMS ionization process, the relative changes of group intensities and the evolution of Si/C and

294   Si/O in $C_xH_yO_zSi_n$ over different PA may be attributed to the evolution of cVMS when oxidized by the OH

295   radicals. The initial step of OH radical oxidation is H abstraction from the methyl groups on the -Si-O- ring

296   of the cVMS to form Si-containing radicals, which may generate OH and CH_2OH substitution products, such

297   as silanol and silyl methanol (Wu and Johnston, 2016; Alton and Browne, 2020). Such Si-containing products

298   may partition into SOA and result in an appearance of $C_xH_yO_zSi_n$ ions in the AMS mass spectra. Notably, it

299   was reported that one of oxidation products of D5, 1- hydroxynonamethylcyclopentasiloxane (D_4TOH), has

300   been detected in ambient particulate matter (Milani et al., 2021). At low PA, some oxygen-containing

301   functional groups (-CH_2OH/-COOH/-OH), which were formed by the reaction of methyl groups in cVMS

302   with OH, resulted in a small Si/O ratio (D5: 0.53; D6: 0.72) compared to that (1.0) in cVMS. With increasing

303   PA, these functional groups (-CH_2OH/-COOH/-OH) may dissociate, leading to an increase in the Si/O ratio.

304   The Si-O bond breaking may mainly happen at high OH exposures, and it may occur after the cleavage of

305   S-C bonds (Rücker and Kümmerer, 2015). According to the previous study of Wu and Johnston(2017), some

306   ring-opened products were generated from the reaction of D5 with OH radicals, necessarily requiring the

307   cleavage of Si-O bonds. The Si-O bond cleavage from the OH radical attack may reduce the number of O

308   atoms, leading to an increase of Si/O at high PA. The continued breaking of Si-O bonds would lead to

309   fragmentation and more volatile products, which caused lower SOA yield and $C_xH_yO_zSi_n$ fraction at longer
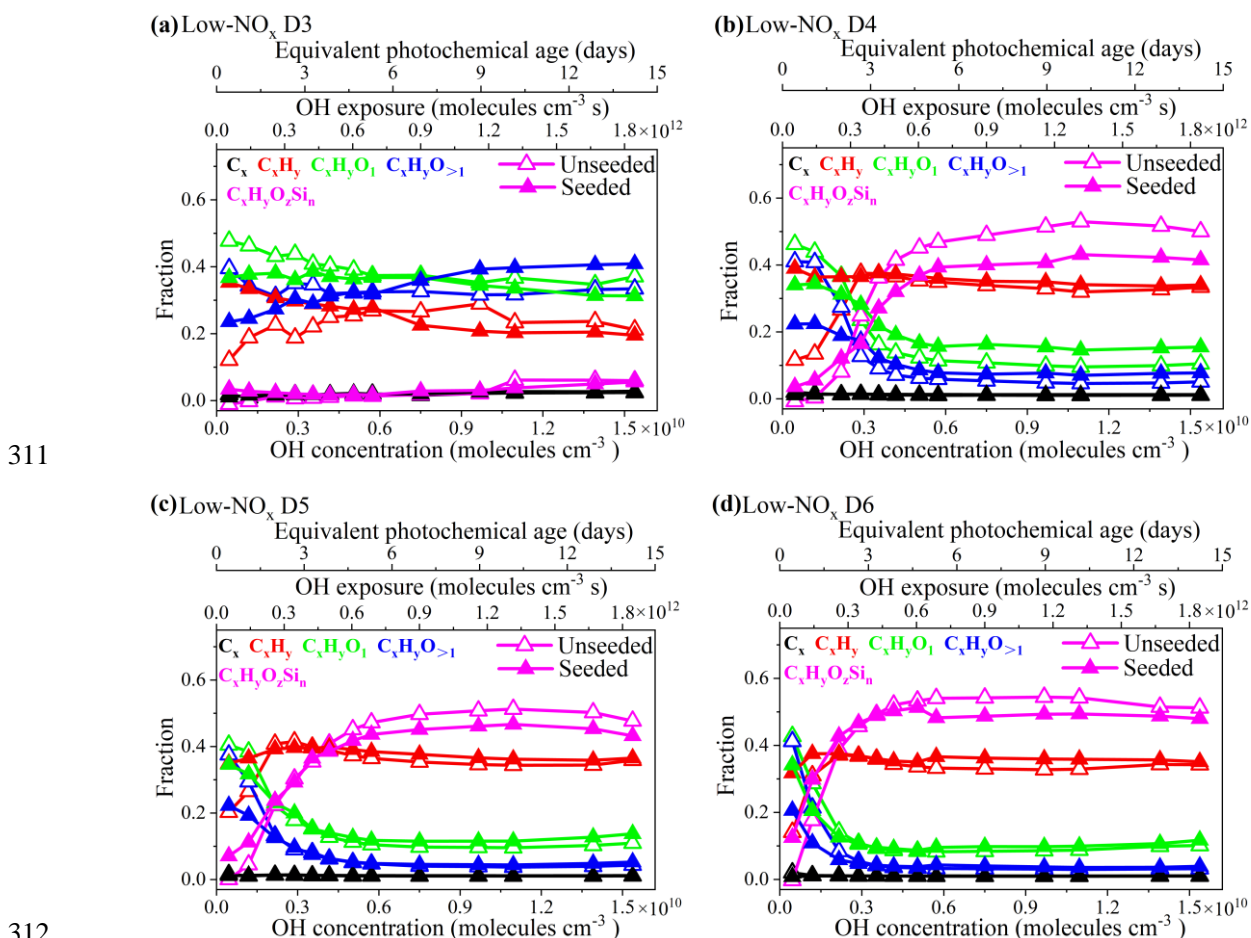
310   PA (Figs. 1 and 3).

Figure 3. Fraction of C_x, C_xH_y, $C_xH_yO_1$, $C_xH_yO_{>1}$ and $C_xH_yO_zSi_n$ ion groups for SOA derived from the

oxidation of cVMS (**a-d**) by OH radicals at different photochemical ages under low-NO_x conditions.

Empty and solid triangles represent experimental data under unseeded and seeded conditions, respectively.

317   As shown in Fig. 3, the presence of seeds led to some changes in the evolution trends of ion groups in the

318   AMS spectra. For instance, the initial fraction of C_xH_y in seeded experiments was larger than that in unseeded

319   experiments, which may be related to the volatility of species containing C_xH_y that may be more easily

320   deposited in the presence of seeds, whereas $C_xH_yO_1$ and $C_xH_yO_{>1}$ exhibited opposite changes. The presence

321   of seeds led to larger initial and smaller steady-state $C_xH_yO_zSi_n$ fractions than those in unseeded experiments.

322   Regardless of the presence of seeds, C_xH_y, $C_xH_yO_1$ and $C_xH_yO_{>1}$ mainly contributed to the composition of

323   all cVMS SOA at initial OH radicals oxidation, but D4-D6 SOA primarily consisted of C_xH_y and $C_xH_yO_zSi_n$

324   after 6 equivalent days.

3.2.2 Compositions of SOA under high-NO_x conditions.

326   Figure S9 shows the HR-ToF-AMS mass spectra of cVMS SOA from unseeded experiments under high-

327   NO_x conditions at OH exposures of 9.0×10^{11} molecules cm^{-3} s (~6.9 d). Compared to that under low-NO_x

328   conditions (Figs. 2 and S7), there was one additional N-containing group (N_mO_z) in the SOA mass spectra

329   under high-NO_x conditions, which accounted for 16%-31%. For the mass spectra of D3-D6 SOA originating

330   from unseeded experiments under high-NO_x conditions in Fig. S9, the dominating peaks of the N_mO_z family

331   were m/z 30 (NO^+) and m/z 46 (NO_2^+). The common main peaks were located at m/z 30 (NO^+) for cVMS

332   SOA, m/z 44 (CO_2^+) for D3-D4 SOA, and m/z 46 (NO_2^+) for D4-D6 SOA. In addition, there were other

333   primary peaks at m/z 29 (CHO^+) for D4 SOA, while m/z 15 (CH_3^+) and m/z 28 (CO^+) for D5-D6 SOA. The

334   m/z 28 (CO^+), similar with m/z 44 (CO_2^+), is considered as a tracer for organic acids (Ng et al., 2010). In the

335   mass spectra for D3-D6 SOA under high-NO_x conditions, the presence of NO^+ (m/z 30) and NO_2^+ (m/z 46)

336   illustrated the formation of organic or inorganic nitrates in SOA (Ng et al., 2007b; Zhao et al., 2018).

337   For the $C_xH_yO_zSi_n$ group in the D4 SOA mass spectrum under high-NO_x conditions, the dominating peaks

338   and their formulas were same as those under low-NO_x conditions. For the $C_xH_yO_zSi_n$ group in D5 SOA, in

339   addition to two typical peaks at m/z 327 and 329 in the low-NO_x experiments, there was another prominent

340   peak at m/z 328, with a formula $C_8H_{12}O_5Si_5$. The $C_xH_yO_zSi_n$ group in D6 SOA had three typical peaks at m/z

341   73 (C_3H_9Si), m/z 387 ($C_8H_{23}O_8Si_5^+$) and m/z 401 ($C_9H_{21}O_{10}Si_4^+$). For the $C_xH_yO_zSi_n$ groups in cVMS SOA,

342   there was little difference in the x, y, z and n value assignment of $C_xH_yO_zSi_n$ peaks in SOA generated under

343   low-NO_x and high-NO_x conditions, suggesting the formation of similar Si-containing oxidation products.

344   For cVMS SOA under high-NO$_x$ conditions, the evolution of family groups as a function of OH exposure

345   was summarized in Fig. S10. The dominated composition at initial stage was C$_x$H$_y$O$_{>1}$ groups for D3-D6

346   SOA. At equivalent days larger than 6, D3 SOA primarily consisted of C$_x$H$_y$O$_{>1}$, N$_m$O$_z$ and C$_x$H$_y$O$_1$ groups,

347   while D4-D6 SOA was mainly composed of C$_x$H$_y$O$_z$Si$_n$, N$_m$O$_z$, C$_x$H$_y$O$_1$, C$_x$H$_y$ and C$_x$H$_y$O$_{>1}$ groups. Figure

348   S10 also shows influences of seeds on the evolution of family groups under high-NO$_x$ conditions. It was

349   observed that all groups in D3-D6 SOA displayed similar change trends regardless of the existence of seeds.

350   As shown in Fig. S11, the trend of the weighted values of the atomic ratio Si/O in the C$_x$H$_y$O$_z$Si$_n$ groups at

351   different photochemical ages under high-NO$_x$ conditions was similar to that in low-NO$_x$ experiments.

352   However, the Si/C ratios remained almost unchanged, and were close to the initial value (0.5) in cVMS. This

353   may be attributed to possible suppression of cleavage of methyl groups from the -Si-O- ring of the cVMS

354   under high-NO$_x$ conditions.

4 Conclusions and implications

356   The yields and compositions of SOA generated from the photooxidation of four cVMS (D3-D6) with OH

357   radicals were investigated using an oxidation flow reactor. cVMS SOA yields exhibited an overall increasing

358   trend with PA, and their values gradually increased with cVMS from D3 to D6. SOA formations depended

359   on NO$_x$, as shown by smaller SOA yields under high-NO$_x$ conditions. Ammonium sulfate seeds significantly

360   enhanced SOA yields of D3-D5 at short PA under high-NO$_x$ conditions. The SOA mass spectra showed that

361   Si-containing species were one of main chemical compositions at PA of >6 days.

362   To evaluate the potential contributions of cVMS to SOA formation in the atmosphere, global SOA

363   concentrations produced from cVMS were estimated according to the cVMS SOA yields measured in this

364   work and using the cVMS concentrations reported from multiple studies, which were listed in Table S6.

365   Here, the high-NO$_x$ SOA yields under the seeded conditions at 8.5 equivalent days (D3: 0.028; D4: 0.122;

366   D5: 0.441; D6: 0.792) are employed in the calculation of cVMS SOA concentrations at urban sites, while

367   the low-NO$_x$ SOA yields under the unseeded conditions at 14.2 equivalent days (D3: 0.148; D4: 0.556; D5:

368   0.805; D6: 0.975) are used to estimate cVMS SOA at background and polar sites. The SOA formation from

369   the reaction of cVMS with OH would always occur when the airmass is transported from urban aeras to low-

370   NO$_x$ sites such as rural, forested, and polar regions. To simplify the estimation process, the SOA yields at

371   the maximum equivalent days (8.5 days) here were used for the calculation of SOA generated by cVMS

372   from urban areas, although 8.5 days are longer for the residence time of an airmass in an urban area.

373   It should be noted that OH concentrations and exposures have different effects on the reaction systems,

374   leading to different SOA yields. OH concentration determines the cVMS+OH reaction rate and therefore the

375   instantaneous cVMS SOA yield. In contrast, OH exposure of cVMS determines the time-integrated, or

376   cumulative, cVMS SOA yield. For any OH concentration, if a cVMS is exposed to the OH for a short period

377   of time, the cumulative SOA yield over the short exposure time will be small. From this perspective,

378   exposure is a more relevant factor to atmospheric conditions because SOA yield under such conditions

379   should be an integration of instantaneous yields over the lifetime of a precursor compound in the atmosphere.

380   Hence, one can argue that exposure experiments such as ours, simulating exposure in the real atmosphere,

381   that were conducted using OFR, should be more suitable for application to the ambient atmosphere.

382   Nevertheless, the interchanges between OH concentrations and exposures have to be considered due to

383   experimental limitations, especially an inability to carry out long-time (multiple days) experiments. When

384   extrapolating the laboratory data to the real atmosphere, it is necessary to consider atmospherically relevant

385   OH concentrations and exposures. Charan et al. (2022) have claimed that D5 SOA yields are strongly

386   dependent on both OH concentrations and exposures, implying the simultaneous effects of OH

387   concentrations and reaction time on SOA yields. OH exposures in this work were 0.05-1.85×10^{12} molecules

388 cm^{-3} s, which was within atmospheric OH exposure range of cVMS when considering half-lives (6-30 days)

389 of cVMS and average OH concentration (1.5×10^6 molecules cm^{-3}) in the atmosphere. Although there may

390 be some uncertainties in extrapolating our results to the real atmosphere, such as larger cVMS concentrations

391 and SOA yields, these extrapolations may still provide an estimation for understanding the SOA potential of

392 cVMS.

393   Figure 4 shows the global concentration distribution of SOA from four cVMS (D3-D6) at 36 sites

394 worldwide estimated by the Equation 4,

$$C_{\text{cVMS-SOA}} = C_{\text{cVMS}} \times \frac{\Delta C_{\text{cVMS}}}{C_{\text{in-cVMS}}} \times Y \tag{4}$$

396 where C_{cVMS} and $C_{\text{cVMS-SOA}}$ are the mass concentration of cVMS reported from literatures and cVMS SOA

397 estimated in global sites, respectively; $C_{\text{in-cVMS}}$ and ΔC_{cVMS} are the mass concentration of initial and lost

398 cVMS at the selected equivalent days during the experiments of this work, respectively (Table S7); Y is the

399 cVMS SOA mass yields mentioned above. It was noted that the estimations from the Equation 4 were based

400 on assumptions that the lost cVMS ratio is not affected by the cVMS concentration and the background

401 $C_{\text{cVMS-SOA}}$ is zero. Table S6 summarizes the details regarding sites and concentrations of cVMS SOA. The

402 derived concentrations of cVMS SOA varies significantly among urban, background and polar sites. The

403 total cVMS SOA concentrations in urban areas are the highest, up to 1324 ng/m^3. They are 18.9-428 and

404 13.8-138.8 ng/m^3 for background and Arctic sites, respectively. cVMS SOA concentrations in urban regions

405 of Asia (sites 29-36) and Europe (sites 26-28) are generally larger than that of North America (sites 20-25).

406 In China, the total cVMS SOA concentrations in urban sites range from 15.5 to 1324 ng/m^3. The main

407 precursors of cVMS SOA are different among Chinese cities. For three cities along the southeast coast of

408 China (Guangzhou, Macau and Foshan), the dominant precursors of cVMS SOA are D3 and D4, which are

409 related to industrial emissions of these two siloxanes in this region (Wang et al., 2001). For Dalian in China,

410   mainly D5 and D6 contribute to cVMS SOA, which have the highest concentrations among all sites. This

411   can be attributed to the industrial production of D5 and D6 and the use of personal care products in Dalian

412   (Li et al., 2020). In the other Chinese urban areas with reported cVMS concentrations (Lhasa, Golmud,

413   Kunming and Yantai), the total cVMS SOA concentrations are considerably smaller than those in the urban

414   areas above, with D5 acting as the main precursor, which may be ascribed to the relatively low population

415   densities in these cities (Wang et al., 2018).
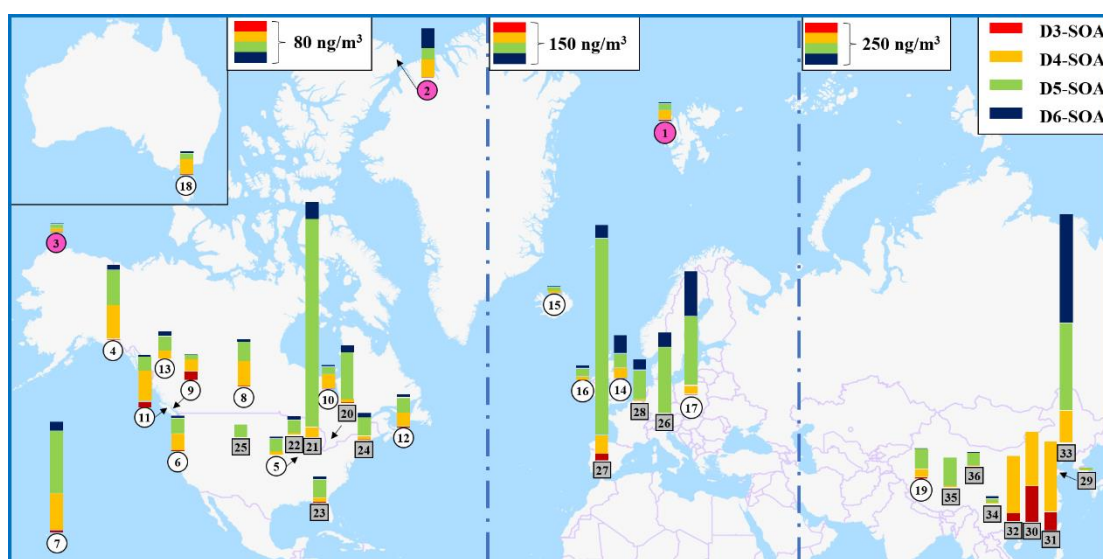
416

417   Figure 4. Global concentrations of cVMS SOA (ng/m^3) on the basis of the cVMS concentrations

418   reported from multiple studies and the cVMS SOA yields measured in this work. The numbers of polar,

419   background and urban sites are enclosed in pink, white circles and gray boxes, respectively. The details

420   about cVMS and SOA concentrations at different sites were summarized in Table S6 of the Supplement.

421

422   At urban sites in Europe and North America, cVMS SOA concentrations are reported in the range of 138-

423   813 ng/m^3 and 22.9-437 ng/m^3, respectively. Among these cVMS, D5 is the main contributor to cVMS SOA

424   at these locations, averaging 80.1% of total cVMS SOA. This contribution is higher than that (73.6%) at

425   Chinese urban sites. For instance, D5 SOA is calculated to be 684 ng/m^3 in Catalan, Spain, 387 ng/m^3 in

426   Chicago, USA, 229 ng/m^3 in Zurich, Switzerland and 99 ng/m^3 in Paris, France, where there are high levels

427   of economic activities and high population densities. These results suggest that personal care products as a

428   main source of D5 may be the most important anthropogenic origins of Si-containing SOA in Europe and

429   North America. It was noted that the D5 SOA concentration (13.38-683.57 ng/m^3) estimated here is far more

430   than that (0.016-0.206 ng/m^3) reported by Milani et al. (2021), who obtained their data using semi-quantified

431   concentrations of D$_4$TOH (first-generation D5 SOA product) extracted from PM$_{2.5}$ samples in Atlanta and

432   Houston. The difference may be mainly attributed to the missing analysis of multi-generation SOA products

433   or dimers (Wu and Johnston, 2016, 2017).   Pennington et al. (2021) utilized the developed CMAQ model

434   to investigate the concentration of D5 SOA in the urban area of Los Angeles, and the model data (21 ng/m^3)

435   was within these D5 SOA concentrations estimated here.

436   At background and Arctic sites, cVMS SOA are primarily derived from D4 and D5. The background sites

437   are located in mountains, rural areas, forested areas, lakes and at high altitudes. The three highest cVMS

438   SOA concentrations at background sites are located at Kosetice in the Czech Republic (428 ng/m^3), Hilo,

439   Hawaii, USA (203 ng/m^3) and Tibetan Plateau in China (174 ng/m^3), where the contribution percentages of

440   SOA from both D4 and D5 are 62.6%, 90.3% and 93.4%, respectively. The cVMS SOA concentrations at

441   the Little Fox Lake site in Yukon, Canada is the highest (138.8 ng/m^3) among the four locations in the Arctic,

442   91% of which is accounted for by both D4 and D5 SOA. The dominance of D4 and D5 SOA in both

443   background and the Arctic regions highlights their persistence in atmosphere and the potential for long-range

444   atmospheric transport.

445   Furthermore, global concentration distribution of Si-containing SOA estimated for the four cVMS (D3-

446   D6) at 36 sites worldwide is also presented in Table S6, which clearly shows the global importance of Si in

447   SOA with the estimated percentages of cVMS SOA that contains the Si element. For example, up to 49.2%

448 and 31.2% of cVMS SOA contained Si elements in background and urban sites, respectively. These results

449 are similar to the summary observations that reported percentages of aerosols with a Si mole fraction >0.01

450 (%) at different sites (Bzdek et al., 2014). The above results demonstrated that Si is a frequent component of

451 SOA in background and urban areas.

452 The global annual production of D4, D5 and D6 is about 1, 0.1 and 0.01 $Tg \cdot yr^{-1}$, respectively, and 90% of

453 these cVMS is eventually released into the atmosphere (Li et al., 2020; Genualdi et al., 2011; Wang et al.,

454 2013; Sakurai et al., 2019). Based on the results shown in Fig. 4, the annual production of cVMS (D4-D6)

455 SOA was estimated to be 0.16 $Tg \cdot yr^{-1}$, which was about 5.5% of SOA (2.9 $Tg \cdot yr^{-1}$) produced from mobile

456 source emissions in the USA and 5-8 times of SOA generated by Athabasca oil sands (0.02-0.03 $Tg \cdot yr^{-1}$, one

457 of the largest sources of anthropogenic secondary organic aerosols in North America) (Tkacik et al., 2014;

458 Liggio et al., 2016). Moreover, it was also 0.8% and 2.3% of isoprene-SOA (20 $Tg \cdot yr^{-1}$) and monoterpenes-

459 SOA (7 $Tg \cdot yr^{-1}$) (typical biogenic SOA), respectively, indicating the potential importance of cVMS SOA

460 (Jokinen et al., 2015). While these cVMS SOA sources may seem small, they can make substantially higher

461 contributions to ambient air SOAs in population centers where cVMS compounds are primarily used.

462

463 **Author contributions**

464 CH designed and conducted all experiments; CH and HY analyzed the data and prepared the paper with

465 contributions from KL, PL, JL, AL and SML. SML supervised the project.

466

467 **Competing interests**

468 The authors declare that they have no conflict of interest.

469 **Acknowledgements**

References

Ahrens, L., Harner, T., and Shoeib, M.: Temporal Variations of Cyclic and Linear Volatile Methylsiloxanes in the Atmosphere Using Passive Samplers and High-Volume Air Samplers, Environ. Sci. Technol., 48, 9374-9381, https://doi.org/10.1021/es502081j, 2014.

Allen, R., Kochs, P., and Chandra, G.: Industrial Organosilicon Materials, Their Environmental Entry and Predicted Fate, Springer, 3, 1-25, https://doi.org/10.1007/978-3-540-68331-5_1, 1997.

Alton, M. and Browne, E.: Atmospheric Chemistry of Volatile Methyl Siloxanes: Kinetics and Products of Oxidation by OH Radicals and Cl Atoms, Environ. Sci. Technol., 54, 5992-5999, https://dx.doi.org/10.1021/acs.est.0c01368, 2020.

Alton, M. W. and Browne, E. C.: Atmospheric Degradation of Cyclic Volatile Methyl Siloxanes: Radical Chemistry and Oxidation Products, ACS Environ. Au, XXX, XXX-XXX, https://doi.org/10.1021/acsenvironau.1c00043, 2022.

Atkinson, R.: Kinetics of the Gas-Phase Reactions of a Series of Organosilicon Compounds with OH and NO_3 Radicals and O_3 at 297 ± 2 K, Environ. Sci. Technol., 25, 863-866, https://doi.org/10.1021/es00017a005, 1991.

Bein, K., Zhao, Y., Wexler, A., Johnston, M.: Speciation of Size-Resolved Individual Ultrafine Particles in Pittsburgh, Pennsylvania, J. Geophys. Res., 110, D07S05, https://doi.org/10.1029/2004jd004708, 2005.

Berndt, T., Richters, S., Jokinen, T., Hyttinen, N., Kurtén, T., Otkjaer, R., Kjaergaard, H., Stratmann, F., Herrmann, H., Sipilä, M., Kulmala, M., and Ehn, M.: Hydroxyl Radical-Induced Formation of Highly Oxidized Organic Compounds, Nat. Commun., 7, 1-8, https://doi.org/10.1038/ncomms13677, 2016.

Bruns, E., Haddad, I., Keller, A., Klein, F., Kumar, N., Pieber, S., Corbin, J., Slowik, J., Brune, W., Baltensperger, U., and Prévôt, A.: Inter-Comparison of Laboratory Smog Chamber and Flow Reactor Systems on Organic Aerosol Yield and Composition, Atmos. Meas. Tech., 8, 2315-2332, https://doi.org/10.5194/amt-8-2315-2015, 2015.

Bzdek, B., Horan, A., Pennington, M., Janechek, N., Baek, J., Stanier, C., and Johnston, M.: Silicon is a Frequent

Component of Atmospheric Nanoparticles, Environ. Sci. Technol., 48, 11137-11145, https://doi.org/10.1021/es5026933, 2014.

Canada, E. C. a. H.: https://www.ec.gc.ca/ese-ees/FC0D11E7-DB34-41AA-B1B3-E66EFD8813F1/batch2_540-97-6_en.pdf last access: 9 February 2022, 2008.

Chan, A., Kautzman, K., Chhabra, P., Surratt, J., Chan, M., Crounse, J., Kürten, A., Wennberg, P., Flagan, R., and Seinfeld, J.: Secondary Organic Aerosol Formation from Photooxidation of Naphthalene and Alkylnaphthalenes: Implications for Oxidation of Intermediate Volatility Organic Compounds (IVOCs), Atmos. Chem. Phys., 9, 3049-3060, https://doi.org/10.5194/acp-9-3049-2009, 2009.

Chandramouli, B., Kamens, R.: The Photochemical Formation and Gas-Particle Partitioning of Oxidation Products of Decamethyl Cyclopentasiloxane and Decamethyl Tetrasiloxane in the Atmosphere, Atmos. Environ., 35, 87-95, https://doi.org/10.1016/S1352-2310(00)00289-2, 2001.

Charan, S., Huang, Y., Buenconsejo, R., Li, Q., Cocker Iii, D., and Seinfeld, J.: Secondary Organic Aerosol Formation from the Oxidation of Decamethylcyclopentasiloxane at Atmospherically Relevant OH Concentrations, Atmos. Chem. Phys., 22, 917-928, https://doi.org/10.5194/acp-22-917-2022, 2022.

Coggon, M., McDonald, B., Vlasenko, A., Veres, P., Bernard, F., Koss, A., Yuan, B., Gilman, J., Peischl, J., Aikin, K., DuRant, J., Warneke, C., Li, S.-M., and Gouw, J.: Diurnal Variability and Emission Pattern of Decamethylcyclopentasiloxane (D5) from the Application of Personal Care Products in Two North American Cities, Environ. Sci. Technol., 52, 5610-5618, https://doi.org/10.1021/acs.est.8b00506, 2018.

EUR-Lex: https://eur-lex.europa.eu/legal-content/EN/TXT/?uri=uriserv:OJ.L_.2018.006.01.0045.01.ENG&toc=OJ:L:2018:006:TOCECHA, last access: 25 November 2021, 2018.

Farasani, A. and Darbre, P.: Exposure to Cyclic Volatile Methylsiloxanes (cVMS) Causes Anchorage-Independent Growth and Reduction of BRCA1 in Non-Transformed Human Breast Epithelial Cells, J. Appl. Toxicol., 37, 454-461, https://doi.org/10.1002/jat.3378, 2017.

Genualdi, S., Harner, T., Cheng, Y., Macleod, M., Hansen, K., Egmond, R., Shoeib, M., and Lee, S.: Global Distribution of Linear and Cyclic Volatile Methyl Siloxanes in Air, Environ. Sci. Technol., 45, 3349-3354, https://doi.org/10.1021/es200301j, 2011.

Glasius, M. and Goldstein, A.: Recent Discoveries and Future Challenges in Atmospheric Organic Chemistry, Environ. Sci. Technol., 50, 2754-2764, https://doi.org/10.1021/acs.est.5b05105, 2016.

Guo, J., Zhou, Y., Cui, J., Zhang, B., and Zhang, J.: Assessment of Volatile Methylsiloxanes in Environmental

528 Matrices and Human Plasma, Sci. Total. Environ., 668, 1175-1182,

529 https://doi.org/10.1016/j.scitotenv.2019.03.092, 2019.

530 Huang, Y., Coggon, M., Zhao, R., Lignell, H., Bauer, M., Flagan, R., and Seinfeld, J.: The Caltech Photooxidation

531 Flow Tube reactor: Design, Fluid Dynamics and Characterization, Atmos. Meas. Tech., 10, 839-867,

532 https://doi.org/10.5194/amt-10-839-2017, 2017.

533 Janechek, N., Hansen, K., and Stanier, C.: Comprehensive Atmospheric Modeling of Reactive Cyclic Siloxanes

534 and their Oxidation Products, Atmos. Chem. Phys., 17, 8357-8370, https://doi.org/10.5194/acp-17-8357-2017,

535 2017.

536 Janechek, N., Marek, R., Bryngelson, N., Singh, A., Bullard, R., Brune, W., and Stanier, C.: Physical Properties

537 of Secondary Photochemical Aerosol from OH Oxidation of a Cyclic Siloxane, Atmos. Chem. Phys., 19, 1649-

538 1664, https://doi.org/10.5194/acp-19-1649-2019, 2019.

539 Jokinen, T., Berndt, T., Makkonen, R., Kerminen, V., Junninen, H., Paasonen, P., Stratmann, F., Herrmann, H.,

540 Guenther, A., Worsnop, D., Kulmala, M., Ehn, M., and Sipilä, M.: Production of Extremely Low Volatile

541 Organic Compounds from Biogenic Emissions: Measured Yields and Atmospheric Implications, Proc. Natl.

542 Acad. Sci. U S A., 112, 7123-7128, https://doi.org/10.1073/pnas.1423977112, 2015.

543 Kierkegaard, A. and McLachlan, M.: Determination of Linear and Cyclic Volatile Methylsiloxanes in Air at a

544 Regional Background Site in Sweden, Atmos. Environ., 80, 322-329,

545 https://doi.org/10.1016/j.atmosenv.2013.08.001, 2013.

546 Kim, J. and Xu, S.: Quantitative Structure-Reactivity Relationships of Hydroxyl Radical Rate Constants for Linear

547 and Cyclic Volatile Methylsiloxanes, Environ. Toxicol. Chem., 36, 3240-3245, https://doi.org/10.1002/etc.3914,

548 2017.

549 Kim, J., Mackay, D., and Whelan, M.: Predicted Persistence and Response Times of Linear and Cyclic Volatile

550 Methylsiloxanes in Global and Local Environments, Chemosphere, 195, 325-335,

551 https://doi.org/10.1016/j.chemosphere.2017.12.071, 2018.

552 Krogseth, I., Zhang, X., Lei, Y., Wania, F., and Breivik, K.: Calibration and Application of a Passive Air Sampler

553 (XAD-PAS) for Volatile Methyl Siloxanes, Environ. Sci. Technol., 47, 4463-4470,

554 https://doi.org/10.1021/es400427h, 2013a.

555 Krogseth, I., Kierkegaard, A., McLachlan, M., Breivik, K., Hansen, K., and Schlabach, M.: Occurrence and

556 Seasonality of Cyclic Volatile Methyl Siloxanes in Arctic Air, Environ. Sci. Technol., 47, 502-509,

557 https://doi.org/10.1021/es3040208, 2013b.

558 Lambe, A., Chhabra, P., Onasch, T., Brune, W., Hunter, J., Kroll, J., Cummings, M., Brogan, J., Parmar, Y.,

559 Worsnop, D., Kolb, C., and Davidovits, P.: Effect of Oxidant Concentration, Exposure Time, and Seed Particles

560 on Secondary Organic Aerosol Chemical Composition and Yield, Atmos. Chem. Phys., 15, 3063-3075,

561 https://doi.org/10.5194/acp-15-3063-2015, 2015.

562 Lambe, A., Ahern, A., Williams, L., Slowik, J., Wong, J., Abbatt, J., Brune, W., Ng, N., Wright, J., Croasdale, D.,

563 Worsnop, D., Davidovits, P., and Onasch, T.: Characterization of Aerosol Photooxidation Flow Reactors:

564 Heterogeneous Oxidation, Secondary Organic Aerosol Formation and Cloud Condensation Nuclei Activity

565 Measurements, Atmos. Meas. Tech., 4, 445-461, https://doi.org/10.5194/amt-4-445-2011, 2011.

566 Lambe, A., Massoli, P., Zhang, X., Canagaratna, M., Nowak, J., Daube, C., Yan, C., Nie, W., Onasch, T., Jayne,

567 J., Kolb, C., Davidovits, P., Worsnop, D., and Brune, W.: Controlled Nitric Oxide Production via $O(^1D) + N_2O$

568 Reactions for Use in Oxidation Flow Reactor Studies, Atmos. Meas. Tech., 10, 2283-2298,

569 https://doi.org/10.5194/amt-10-2283-2017, 2017.

570 Lamkaddam, H., Gratien, A., Pangui, E., Cazaunau, M., Varrault, B., and Doussin, J.: High-NO_x Photooxidation

571 of n-Dodecane: Temperature Dependence of SOA Formation, Environ Sci Technol, 51, 192-201,

572 https://doi.org/10.1021/acs.est.6b03821, 2017.

573 Lee, A., Hayden, K., Herckes, P., Leaitch, W., Liggio, J., Macdonald, A., and Abbatt, J.: Characterization of

574 Aerosol and Cloud Water at a Mountain Site During WACS 2010: Secondary Organic Aerosol Formation

575 through Oxidative Cloud Processing, Atmos. Chem. Phys., 12, 7103-7116, https://doi.org/10.5194/acp-12-

576 7103-2012, 2012.

577 Li, K., Liggio, J., Lee, P., Han, C., Liu, Q., and Li, S.-M.: Secondary Organic Aerosol Formation from α-Pinene,

578 Alkanes, and Oil Sand-Related Precursors in a New Oxidation Flow Reactor, Atmos. Chem. Phys., 19, 9715-

579 9731, https://doi.org/10.5194/acp-19-9715-2019, 2019a.

580 Li, K., Liggio, J., Han, C., Liu, Q., Moussa, S., Lee, P., and Li, S.-M.: Understanding the Impact of High-NO_x

581 Conditions on the Formation of Secondary Organic Aerosol in the Photooxidation of Oil Sand-Related

582 Precursors, Environ. Sci. Technol., 53, 14420-14429, https://doi.org/10.1021/acs.est.9b05404, 2019b.

583 Li, Q., Lan, Y., Liu, Z., Wang, X., Wang, X., Hu, J., and Geng, H.: Cyclic Volatile Methylsiloxanes (cVMSs) in

584 the Air of the Wastewater Treatment Plants in Dalian, China-Levels, Emissions, and Trends, Chemosphere, 256,

585 1-8, https://doi.org/10.1016/j.chemosphere.2020.127064, 2020.

586 Li, S.-M. and Winchester, J.: Particle Size Distribution and Chemistry of Late Winter Arctic Aerosols, J. Geophys.

587 Res., 95, 13897-13908, https://doi.org/10.1029/J095iD09p13897, 1990.

588 Li, S.-M. and Winchester, J.: Aerosol Silicon and Associated Elements in the Arctic High and Mid-Troposphere,

589 Atmos. Environ., 27, 2907-2912, https://doi.org/10.1016/0960-1686(93)90322-P, 1993.

590 Liggio, J., Li, S.-M., Hayden, K., Taha, Y., Stroud, C., Darlington, A., Drollette, B., Gordon, M., Lee, P., Liu, P.,

591 Leithead, A., Moussa, S., Wang, D., Brien, J., Mittermeier, R., Brook, J., Lu, G., Staebler, R., Han, Y., Tokarek,

592 T., Osthoff, H., Makar, P., Zhang, J., Plata, D., and Gentner, D.: Oil Sands Operations as a Large Source of

593 Secondary Organic Aerosols, Nature, 534, 91-94, https://doi.org/10.1038/nature17646, 2016.

594 Liu, N., Xu, L., and Cai, Y.: Methyl Siloxanes in Barbershops and Residence Indoor Dust and the Implication for

595 Human Exposures, Sci. Total. Environ., 618, 1324-1330, https://doi.org/10.1016/j.scitotenv.2017.09.250, 2018.

596 Mao, J., Ren, X., Brune, W., Olson, J., Crawford, J., Fried, A., Huey, L., Cohen, R., Heikes, B., Singh, H., Blake,

597 D., Sachse, G., Diskin, G., Hall, S., and Shetter, R.: Airborne Measurement of OH Reactivity during INTEX-

598 B, Atmos. Chem. Phys., 9, 163-173, https://doi.org/10.5194/acp-9-163-2009, 2009.

599 McFiggans, G., Mentel, T., Wildt, J., Pullinen, I., Kang, S., Kleist, E., Schmitt, S., Springer, M., Tillmann, R., Wu,

600 C., Zhao, D., Hallquist, M., Faxon, C., Breton, M., Hallquist, A., Simpson, D., Bergström, R., Jenkin, M., Ehn,

601 M., Thornton, J., Alfarra, M., Bannan, T., Percival, C., Priestley, M., Topping, D., and Scharr, A.: Secondary

602 Organic Aerosol Reduced by Mixture of Atmospheric Vapours, Nature, 565, 587-593,

603 https://doi.org/10.1038/s41586-018-0871-y, 2019.

604 Milani, A., Al-Naiema, I., and Stone, E.: Detection of a Secondary Organic Aerosol Tracer Derived from Personal

605 Care Products, Atmos. Environ., 246, https://doi.org/10.1016/j.atmosenv.2020.118078, 2021.

606 Ng, N., Kroll, J., Chan, A., Chhabra, P., Flagan, R., and Seinfeld, J.: Secondary Organic Aerosol Formation from

607 m-Xylene, Toluene, and Benzene, Atmos. Chem. Phys., 7, 3909-3922, https://doi.org/10.5194/acp-7-3909-2007,

608 2007a.

609 Ng, N., Chhabra, P., Chan, A., Surratt, J., Kroll, J., Kwan, A., McCabe, D., Wennberg, P., Sorooshian, A., Murphy,

610 S., Dalleska, N., Flagan, R., and Seinfeld, J.: Effect of NO_x Level on Secondary Organic Aerosol (SOA)

611 Formation from the Photooxidation of Terpenes, Atmos. Chem. Phys., 7, 5159-5174,

612 https://doi.org/10.5194/acp-7-5159-2007, 2007b.

613 Ng, N., Canagaratna, M., Zhang, Q., Jimenez, J., Tian, J., Ulbrich, I., Kroll, J., Docherty, K., Chhabra, P., Bahreini,

614 R., Murphy, S., Seinfeld, J., Hildebrandt, L., Donahue, N., DeCarlo, P., Lanz, V., Prévôt, A., Dinar, E., Rudich,

615 Y., and Worsnop, D.: Organic Aerosol Components Observed in Northern Hemispheric Datasets from Aerosol

616 Mass Spectrometry, Atmos. Chem. Phys., 10, 4625-4641, https://doi.org/10.5194/acp-10-4625-2010, 2010.

617 Peng, Z., Taylor, J., Orlando, J., Tyndall, G., and Jimenez, J.: Organic Peroxy Radical Chemistry in Oxidation

Flow Reactors and Environmental Chambers and their Atmospheric Relevance, Atmos. Chem. Phys., 19, 813-834, https://doi.org/10.5194/acp-19-813-2019, 2019.

Peng, Z., Palm, B., Day, D., Talukdar, R., Hu, W., Lambe, A., Brune, W., and Jimenez, J.: Model Evaluation of New Techniques for Maintaining High-NO Conditions in Oxidation Flow Reactors for the Study of OH-Initiated Atmospheric Chemistry, ACS. Earth. Space. Chem. , 2, 72-86, https://doi.org/10.1021/acsearthspacechem.7b00070, 2018.

Pennington, E., Seltzer, K., Murphy, B., Qin, M., Seinfeld, J., and Pye, H.: Modeling Secondary Organic Aerosol Formation from Volatile Chemical Products, Atmos. Chem. Phys., 21, 18247-18261, https://doi.org/10.5194/acp-21-18247-2021, 2021.

Phares, D., Rhoads, K., Johnston, M., and Wexler, A.: Size-Resolved Ultrafine Particle Composition Analysis 2. Houston, J. Geophys. Res., 108, 1-14, https://doi.org/10.1029/2001jd001212, 2003.

Presto, A., Hartz, K., and Donahue, N.: Secondary Organic Aerosol Production from Terpene Ozonolysis. 2. Effect of NO_x Concentration, Environ. Sci. Technol. , 39, 7046-7054, https://doi.org/10.1021/es050400s, 2005.

Rauert, C., Shoieb, M., Schuster, J., Eng, A., and Harner, T.: Atmospheric Concentrations and Trends of Poly- and Perfluoroalkyl Substances (PFAS) and Volatile Methyl Siloxanes (VMS) over 7 Years of Sampling in the Global Atmospheric Passive Sampling (GAPS) Network, Environ. Pollut., 238, 94-102, https://doi.org/10.1016/j.envpol.2018.03.017, 2018.

Rhoads, K., Phares, D., Wexler, A., Johnston, M.: Size-Resolved Ultrafine Particle Composition Analysis 1. Atlanta, J. Geophys. Res., 108, 1-13, https://doi.org/10.1029/2001jd001211, 2003.

Riipinen, I., Juuti, T., Pierce, J., Petäjä, T., Worsnop, D., Kulmala, M., and Donahue, N.: The Contribution of Organics to Atmospheric Nanoparticle Growth, Nat. Geosci., 5, 453-458, https://doi.org/10.1038/ngeo1499, 2012.

Rücker, C. and Kümmerer, K.: Environmental Chemistry of Organosiloxanes, Chem. Rev., 115, 466-524, https://doi.org/10.1021/cr500319v, 2015.

Safron, A., Strandell, M., Kierkegaard, A., and Macleod, M.: Rate Constants and Activation Energies for Gas-Phase Reactions of Three Cyclic Volatile Methyl Siloxanes with the Hydroxyl Radical, Int. J. Chem. Kinet., 47, 420-428, https://doi.org/10.1002/kin.20919, 2015.

Sakurai, T., Imaizumi, Y., Kuroda, K., Hayashi, T., and Suzuki, N.: Georeferenced multimedia environmental fate of volatile methylsiloxanes modeled in the populous Tokyo Bay catchment basin, Sci Total Environ, 689, 843-853, https://doi.org/10.1016/j.scitotenv.2019.06.462, 2019.

648 Sarrafzadeh, M., Wildt, J., Pullinen, I., Springer, M., Kleist, E., Tillmann, R., Schmitt, S., Wu, C., Mentel, T., Zhao,

649   D., Hastie, D., and Scharr, A.: Impact of NO_x and OH on Secondary Organic Aerosol Formation from β-Pinene

650   Photooxidation, Atmos. Chem. Phys., 16, 11237-11248, https://doi.org/10.5194/acp-16-11237-2016, 2016.

651 Simonen, P., Saukko, E., Karjalainen, P., Timonen, H., Bloss, M., Saksa, P., Rönkkö, T., Keskinen, J., and Maso,

652   M.: A New Oxidation Flow Reactor for Measuring Secondary Aerosol Formation of Rapidly Changing

653   Emission Sources, Atmos. Meas. Tech., 10, 1519-1537, https://doi.org/10.5194/amt-10-1519-2017, 2017.

654 Sommerlade, R., Parlar, H., Wrobel, D , Kochs, P.: Product Analysis and Kinetics of the Gas-Phase Reactions of

655   Selected Organosilicon Compounds with OH Radicals Using a Smog Chamber-Mass Spectrometer System,

656   Environ. Sci. Technol., 27, 2435-2440, https://doi.org/10.1021/es00048a019, 1993.

657 Tang, X., Misztal, P., Nazaroff, W., and Goldstein, A.: Siloxanes Are the Most Abundant Volatile Organic

658   Compound Emitted from Engineering Students in a Classroom, Environ. Sci. Technol. Lett. , 2, 303-307,

659   https://doi.org/10.1021/acs.estlett.5b00256, 2015.

660 Tkacik, D., Lambe, A., Jathar, S., Li, X., Presto, A., Zhao, Y., Blake, D., Meinardi, S., Jayne, J., Croteau, P., and

661   Robinson, A.: Secondary Organic Aerosol Formation from in-Use Motor Vehicle Emissions Using a Potential

662   Aerosol Mass Reactor, Environ. Sci. Technol., 48, 11235-11242, https://doi.org/10.1021/es502239v, 2014.

663 Wang, D.-G., Norwood, W., Alaee, M., Byer, J., and Brimble, S.: Review of Recent Advances in Research on the

664   Toxicity, Detection, Occurrence and Fate of Cyclic Volatile Methyl Siloxanes in the Environment, Chemosphere,

665   93, 711-725, https://doi.org/10.1016/j.chemosphere.2012.10.041, 2013.

666 Wang, X., Schuster, J., Jones, K., and Gong, P.: Occurrence and Spatial Distribution of Neutral Perfluoroalkyl

667   Substances and Cyclic Volatile Methylsiloxanes in the Atmosphere of the Tibetan Plateau, Atmos. Chem. Phys.,

668   18, 8745-8755, https://doi.org/10.5194/acp-18-8745-2018, 2018.

669 Wang, X., Lee, S., Sheng, G., Chan, L., Fu, J., Li, X., Min, Y., and Chan, C.: Cyclic organosilicon compounds in

670   ambient air in Guangzhou, Macau and Nanhai, Pearl River Delta, Appl. Geochemistry, 16, 1447-1454,

671   https://doi.org/10.1016/S0883-2927(01)00044-0, 2001.

672 Wildt, J., Mentel, T., Scharr, A., Hoffmann, T., Andres, S., Ehn, M., Kleist, E., Müsgen, P., Rohrer, F., Rudich, Y.,

673   Springer, M., Tillmann, R., and Wahner, A.: Suppression of New Particle Formation from Monoterpene

674   Oxidation by NO_x, Atmos. Chem. Phys., 14, 2789-2804, https://doi.org/10.5194/acp-14-2789-2014, 2014.

675 Wu, Y. and Johnston, M.: Molecular Characterization of Secondary Aerosol from Oxidation of Cyclic

676   Methylsiloxanes, J. Am. Soc. Mass Spectrom., 27, 402-409, https://doi.org/10.1007/s13361-015-1300-1, 2016.

677 Wu, Y. and Johnston, M.: Aerosol Formation from OH Oxidation of the Volatile Cyclic Methyl Siloxane (cVMS)

678   Decamethylcyclopentasiloxane, Environ. Sci. Technol., 51, 4445-4451,

679   https://doi.org/10.1021/acs.est.7b00655, 2017.

680   Xiao, R., Zammit, I., Wei, Z., Hu, W.-P., MacLeod, M., and Spinney, R.: Kinetics and Mechanism of the Oxidation

681   of Cyclic Methylsiloxanes by Hydroxyl Radical in the Gas Phase: An Experimental and Theoretical Study,

682   Environ. Sci. Technol., 49, 13322-13330, https://doi.org/10.1021/acs.est.5b03744, 2015.

683   Xu, S., Warner, N., Nizzetto, P., Durham, J., and McNett, D.: Long-Range Transport Potential and Atmospheric

684   Persistence of Cyclic Volatile Methylsiloxanes Based on Global Measurements, Chemosphere, 228, 460-468,

685   https://doi.org/10.1016/j.chemosphere.2019.04.130, 2019.

686   Zhao, D., Schmitt, S., Wang, M., Acir, I., Tillmann, R., Tan, Z., Novelli, A., Fuchs, H., Pullinen, I., Wegener, R.,

687   Rohrer, F., Wildt, J., Scharr, A., Wahner, A., and Mentel, T.: Effects of NO_x and SO_2 on the Secondary Organic

688   Aerosol Formation from Photooxidation of α-Pinene and Limonene, Atmos. Chem. Phys., 18, 1611-1628,

689   https://doi.org/10.5194/acp-18-1611-2018, 2018.

690   Zhou, C., Jang, M., and Yu, Z.: Simulation of SOA Formation from the Photooxidation of Monoalkylbenzenes in

691   the Presence of Aqueous Aerosols Containing Electrolytes under Various NO_x Levels, Atmos. Chem. Phys., 19,

692   5719-5735, https://doi.org/10.5194/acp-19-5719-2019, 2019.

693